scientific reports

Check for updates

OPEN

The effects of teleconnections on water and carbon fluxes in the two South America's largest biomes

Edivaldo A. O. Serrão[1]✉, Rosane B. L. Cavalcante[1], Paulo R. Zanin[1], Renata G. Tedeschi[1], Thomas R. Ferreira[2] & Paulo R. M. Pontes[1]

Ecosystem services provided by terrestrial biomes, such as moisture recycling and carbon assimilation, are crucial components of the water, energy, and biogeochemical cycles. These biophysical processes are influenced by climate variability driven by distant ocean-atmosphere interactions, commonly referred to as teleconnections. This study aims to identify which teleconnections most significantly affect key biophysical processes in South America's two largest biomes: The Amazon and Cerrado. Using 20 years of monthly data on Precipitation (P), Evapotranspiration (ET), Gross Primary Productivity (GPP), and Ecosystem Water Use Efficiency (EWUE), alongside data from six teleconnections (Antarctic Oscillation - AAO, Atlantic Multidecadal Oscillation - AMO, Oceanic Niño Index - ONI, Atlantic Meridional Mode - AMM, North Atlantic Oscillation - NAO, and Pacific Decadal Oscillation - PDO), we developed a multivariate linear model to assess the relative importance of each teleconnection. Additionally, time-lagged Spearman correlations were used to explore relationships between biophysical variables and teleconnections. Our findings indicate that the AMO exerts the strongest influence across all studied variables. Furthermore, ONI and AMM significantly impact precipitation in the northern Amazon, with a 3-month lag in ONI showing positive correlations with ET and GPP. In contrast, a 3-month lag in AMO negatively influences GPP in the southern Amazon and Cerrado, though positive correlations with EWUE were observed in the same region. These insights highlight the complex and regionally varied impacts of teleconnections on South America's largest biomes.

Keywords Biophysical variables, Carbon fluxes, Teleconnections

Terrestrial ecosystems play a key role in the global water and carbon cycle, and the largest natural global flow of carbon is through absorption via photosynthesis[1,2]. The ecological functions of terrestrial ecosystems are mainly reflected in evapotranspiration and Gross Primary Production (GPP)[3]. GPP refers to the total amount of carbon fixed by autotrophs per unit area and time in photosynthesis[4,5]. Worldwide, terrestrial GPP flux corresponds to more than 100 billion tons of carbon annually, mostly in tropical forests and savannahs[2]. Therefore, terrestrial GPP is a fundamental variable for understanding the atmosphere-biosphere interactions and the global carbon cycle, which directly impact and are impacted by climate change. GPP depends on the health of vegetation and the availability of water and energy[6,7].

As one of the largest consuming components of water resources, Evapotranspiration (ET) plays a crucial role in connecting hydrological processes and ecosystems on the Earth's surface and is an important parameter for evaluating heat and water exchange in the soil-surface-atmosphere continuum[3]. However, these exchanges vary in space and time within the same biome[8,9]. Furthermore, ET is coupled to carbon assimilation through GPP, forming the two dominant processes in the global water and carbon cycles[10]. Changes in vegetation photosynthesis relative to water use are captured by the ratio of Gross Primary Productivity (GPP) to evapotranspiration (ET), known as Ecosystem Water Use Efficiency (EWUE)[11]. The EWUE reflects how efficiently an ecosystem converts water into biomass through photosynthesis, providing insights into its capacity to maintain productivity under varying water availability conditions[12]. The Precipitation (P), GPP, ET, and, consequently, EWUE serve as key indicators of environmental changes.

These metrics reflect shifts in ecosystem functioning, water cycle dynamics, and plant productivity, providing insights into how ecosystems respond to climate variability, water availability, and land-use changes. This is

[1]Vale Institute of Technology, Sustainable Development, Belém, Pará, Brazil. [2]Institute of Atmospheric Sciences, Federal University of Alagoas, Maceió, Alagoas, Brazil. ✉email: edivaldo.serrao@pq.itv.org; oliveiraserrao@gmail.com

especially useful in South America's two largest biomes, where there is anthropogenic pressure (deforestation, fires, land grabbing and others) resulting in a loss of biodiversity and ecosystem services[13,14]. In addition, natural climate variability such as ENSO, which drives extreme events, puts even more pressure on ecosystem services.

Changes in energy and water availability affect photosynthetic rates and carbon fixation. These variations in the water and energy balance are also associated in a non-trivial way with ocean-atmosphere couplings, by which climate anomalies can be related to each other at large distances, such as teleconnections[15,16].

Teleconnections control atmospheric dynamics through changes in heat and momentum flux, modulating weather conditions[17,18]. Consequently, teleconnections affect GPP variations over more than 80% of the global vegetated area, with emphasis on El Niño–Southern Oscillation (ENSO), the Pacific Decadal Oscillation (PDO), and the Atlantic Multidecadal Oscillation (AMO)[19–21].

Each teleconnection's importance can vary regionally. For example, the AMO and NAO, located in the Atlantic, control the variability of GPP and P in China[22,23]. Similarly, the Pacific, through the PDO, strongly influences these variables in the USA[24,25] emphasize that interactions and teleconnections drive the variability of various ecosystem services worldwide. However, correlating these indices with environmental variables presents challenges, as the relationships are not always direct or significant[16].

Considering the results of global analysis of teleconnections in the two larger biomes of South America, ENSO shows a negative correlation with GPP in northeastern Cerrado and in central and northeastern Amazon, and a possible positive correlation in the northern Amazon (depending on the study), with different lag time[19,21,26] observed weak but significant correlations (−0.2) between precipitation and ENSO in the northern Amazon, with a lag time of up to 4 months. Similarly[16], identified positive precipitation anomalies in the Cerrado during spring under AMM conditions, corresponding to a lag of 7 months. AMO and ENSO were observed to be the two main teleconnections that affect GPP in the Amazon and Cerrado biomes with lag time between 3 and 6 months, mainly due to the influence on temperature[20]. ENSO also stands out as the main teleconnection impacting the leaf area index (GPP driver) in the eastern Amazon and Cerrado[25]. However, these studies often overlook the regional specificity of teleconnections, meaning that ocean-atmosphere interactions closer to the study area may exert a more pronounced influence or provide faster feedback on environmental variables such as GPP, ET, and P. This localized impact can result in stronger correlations between nearby teleconnections and ecosystem responses, which may differ from the effects of more distant global patterns[15,20,25].

To individualize the coupled effects of various phenomena, it is possible to use relative importance, which can be extracted from various machine learning-based methods, such as Random Forest, Lindeman Merenda and Gold model (LMG), Shapley Additive exPlanations model (SHAP) and others. For example[27], used Random Forest to identify the main drivers of secondary forest growth in the Amazon[28] used the SHAP model and random forest to quantify the importance of drivers of ecosystem sensitivity in China[23] used LMG to identify which teleconnections are most important in controlling the hydroclimatic variables of the Indochina Peninsula. Therefore, this article addresses the following question: What teleconnection has the greatest influence on the variability of P, ET, GPP, and EWUE in the Amazon and Cerrado biomes at a watershed scale?

Results

Climatology of precipitation and biophysical variables

The spatial distribution of the precipitation and biophysical (GPP, ET, and EWUE) variables follows a predominant northwest-southeast climatic pattern, except for the ET, as shown in Fig. 1. The average climatological characteristics of precipitation (Fig. 1A), evapotranspiration (Fig. 1B), GPP (Fig. 1C) and EWUE (Fig. 1D), reflect the energy regime and the prevailing weather systems in South America (SA), as described by[16], and more precisely in the Amazon Basin[9]. For example, the northern and northwestern regions of the Amazon have the highest rainfall (~ 3000 mm). In comparison, the lowest rainfall values (~ 1300–1700 mm) are observed in the southern transition between the Amazon and the Cerrado and in the east of the Cerrado.

Regarding ET (Fig. 1B), the highest ET values (~ 1000–1900 mm) are distributed across the northern Amazon, in the northeastern Amazon-Cerrado transition and in parts of the south-southeastern Amazon. The lowest ET rates (< 400–600 mm) are mainly observed in the Cerrado, in the southern Amazon and in the Andes Mountain.

The GPP (Fig. 1C) shows a similar northwest-southeast spatial pattern to precipitation. The lowest concentration of carbon assimilation (~ 150–280 ktC/km^2/year) is in the Cerrado biome (east of the basins), and lower GPP values (< 150 ktC/km^2/year) are concentrated in the same places with minimum ET, and low EWUE, highlighting the scarcity of biomass.

The central portion and northern parts of the Amazon, in addition to the Cerrado, hold intermediate values (~ 0.36–0.48 ktC mm^{-1} H_2O) of EWUE (Fig. 1D). In comparison, lower values of EWUE (< 0.23 ktC mm^{-1} H_2O) are found in most of the Cerrado basins, especially in the northeastern sector. The northwest of the Amazon shows the best water use efficiency (> 0.48 ktC mm^{-1} H_2O). This indicates low ecosystem water use efficiency in the Amazon ecosystem and the Cerrado in general. This reveals that the ecosystem uses water in various hydroclimatological and biogeochemical processes and not just for plant growth, as observed by[29]. Furthermore, the evapotranspiration product used here does not partition evaporation (soil surface and canopy interception) from vegetation transpiration.

The watersheds in G1 show a seasonal contrast with those in other groups (Fig. 1E). The highest values of EWUE and P in G1 are in April and May, and the lowest are in September and October. For the other groups, the biophysical variables (except for EWUE4) have their highest values at the end of summer and beginning of fall in the Southern Hemisphere (SH) (Feb-Mar) and the lowest between August and September, which is the end of winter and beginning of spring in the SH.

All groups presented a high positive significant (Fig. 1F) correlation (> 0.7) between GPP and ET. The highest correlation was observed in group 4. GPP and P's correlation varies from − 0.07 in G1 to 0.64 in G4. The best correlations for EWUE were with P and ET, as EWUE2 and P2 (0.66) and EWUE1 and ET1(−0.8). Significant

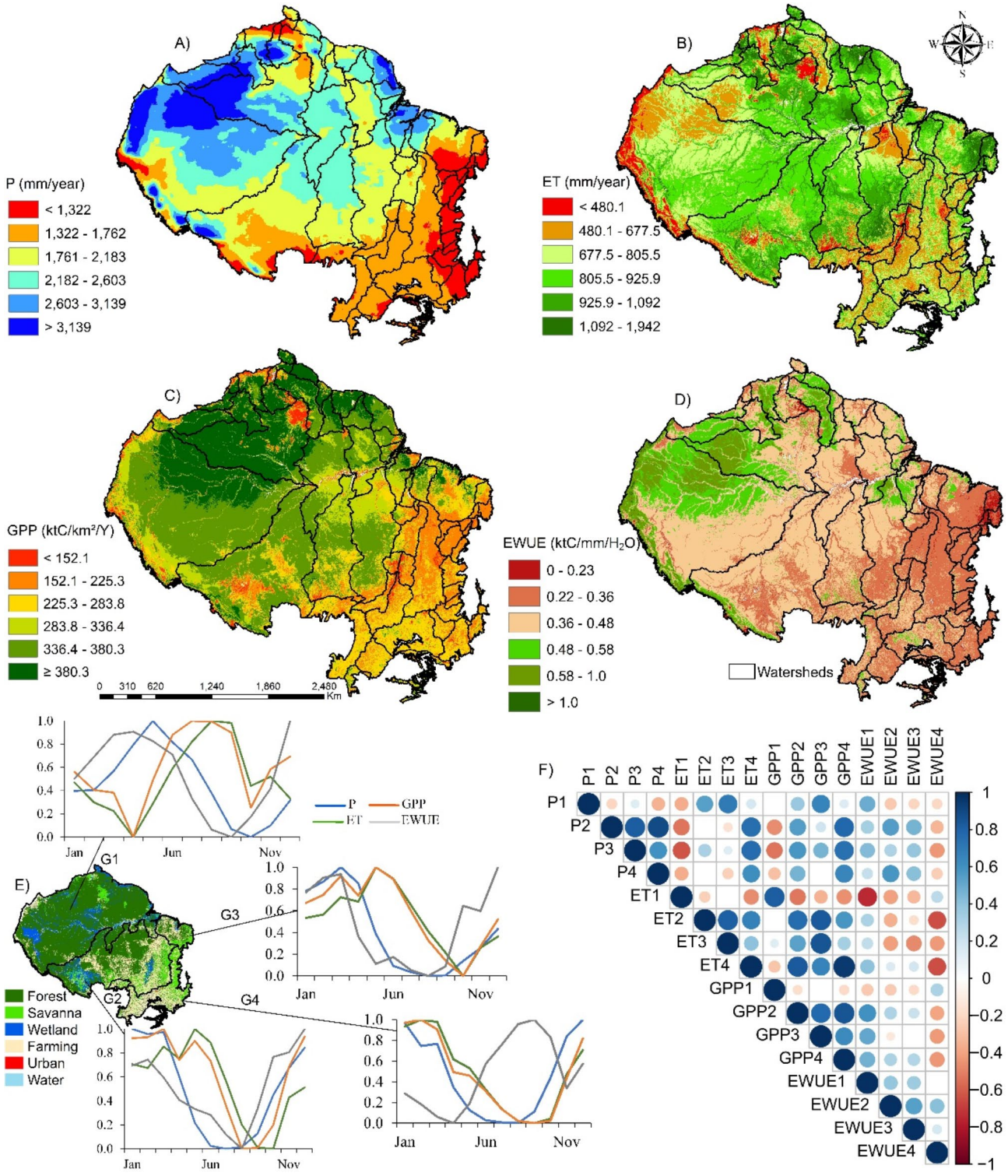

Fig. 1. Long-term spatial pattern of annual Precipitation (P) (**A**); Evapotranspiration (**B**); Gross Primary Productivity (GPP) (**C**); Ecosystem Water Use Efficiency (EWUE) (**D**); (**E**) Land cover change and normalized seasonal variability of P [blue line], ET [green line], GPP [orange line] and EWUE [grey line] by watershed group [e.g. G1, group 1, see methods] (F); Spearman correlation between the monthly precipitation and biophysical variables by watershed group, where the abbreviation of the variable followed by the number indicates the average of the variable for the group [e.g. P1 average monthly precipitation of the watersheds in group 1]; Size of the circle indicates the strength of the correlations ($\alpha < 0.05$), blank spaces indicate that the correlation is not statistically significant. The map was created with ArcGIS Desktop 10.8.1 (https://support.esri.com/en-us/patches-updates/2024/arcgis-desktop-10-8-1-general-component-updates-patch).

correlations were also observed for the same variable between different groups, with the highest values observed between P1 and ET3 (0.7), P3 and ET1 (−0.7), ET2 and GPP3 (0.8), ET4 and P2 (0.7) and EWUE1 and GPP2 (0.7). All correlations and their significance can be seen in Table 1 of the supplementary document.

Contributions of teleconnections to biophysical variables

After applying the LMG algorithm to assess the individual contribution of each teleconnection to precipitation and the biophysical variables (Fig. 2), we found that the AMO emerged as the dominant global contributor across all variables studied. Notably, its influence was strongest on P2 (16.1%), ET4 (18.5%), and GPP2 and GPP4 (17.8% and 18.6%, respectively), highlighting its significant impact on both water and carbon cycle processes. The PDO emerges as the second most influential teleconnection, particularly in groups 2 and 4. Its effect is notable on ET2 (5%), GPP2 (4.5%), ET4 (4.2%), GPP4 (3.2%), and EWUE4 (4.9%), underscoring its significant role in regulating both water and carbon dynamics within these specific groups. In addition, NAO and AAO also contribute to the variability of precipitation and biophysical indicators. Where, NAO contributes more to group 4 (P4, 3.3%; ET and GPP4 equally with 3.5%) and group 2 (P2, 4.5%). On the other hand, the greatest AAO contributions are in group 4 (ET4, 1.8%; GPP4, 1.6%; and EWUE4, 1.3%), group 3 (GPP3, 1.7%), and group 2 (ET2, 1.3%).

Important contributions from ONI and AMM were found in the precipitation of Amazon P1 (13.90% and 13.60%, respectively). ONI also stands out for ET1 (2.6%) and EWUE1 (3.5%) compared to AMM for the same (1.2% and 0.8, respectively) variables. On the other hand, AMM was more important (0.9%) than ONI (0.5%) for GPP1. ONI and AMM exhibit important contributions in several groups such as P3 (2% and 1.7%), ET1 (2.6% and 1.2%), EWUE1 (3.5% and 0.8%), EWUE4 (1.1% and 0.9) and GPP3 (10.5% and 3.5%). Despite this, ONI did not make a strong contribution to GPP in the other groups. This result does not imply that ENSO lacks influence in these regions but rather highlights that teleconnections with longer life cycles, such as the AMO, tend to have a more pronounced impact than the shorter-lived ONI. This suggests that certain teleconnections' persistence and extended effects may overshadow those with more transient patterns.

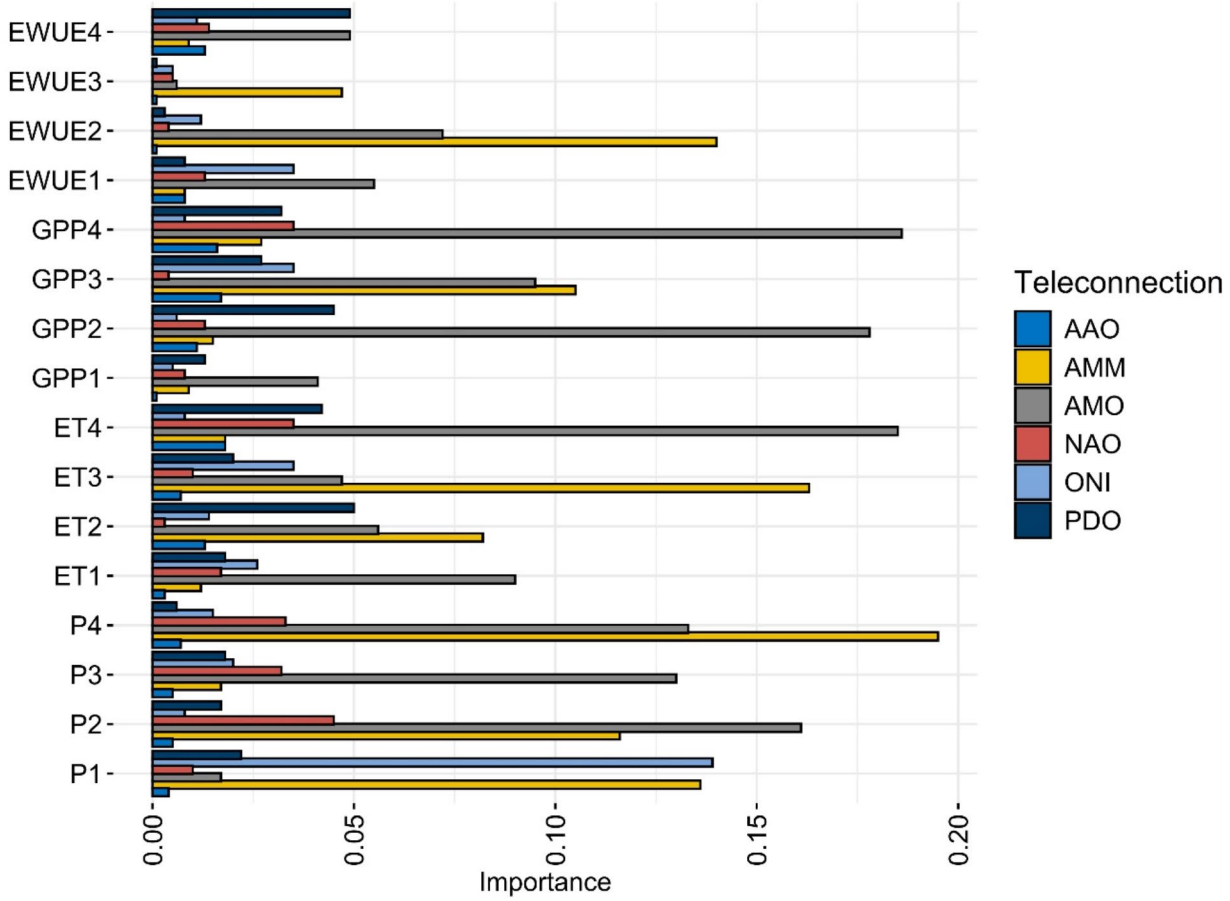

Fig. 2. Relative importance of the teleconnections that control the variability of the monthly timeseries of the precipitation and biophysical indicators in the four basin groups based on LMG values. The figure was created with R 4.3.1 (https://cran.r-project.org/).

Time-lagged effects of teleconnections on precipitation and biophysical variables

For the time-lag analysis, the focus is on the teleconnections with the greatest relative importance (ONI, AMM and AMO). In general, the correlations between AMO (Fig. 3) and the variables three months ahead are more intense than those just one month later. For the one-month lag time, the correlation between AMO and P (Fig. 3a) varies from negative (−0.10 to −0.34) in the northwest (in basins located in G1) to positive (0.10 to 0.24) in the south (in basins located in G2 and G3). Between AMO and GPP the correlation varies from positive in the northeast (including most basins in G3, from 0.25 to 0.34) to negative (−0.1 to −0.24) in the south of the Amazon and Cerrado (including basins in G2 and G4). In the case of ET, 87% of the basins showed significant correlations with AMO (Fig. 3n). With a one-month lag, most basins in groups 1, 2 and 3 had positive (up to 0.34) correlations, while basins in group 4 and parts of group 2 showed negative correlations. As for EWUE, only 3% of the basins showed positive correlations with AMO in group 4. However, in groups 1 and 2, 30% of the basins showed negative (−0.35 to −0.44) correlations.

The correlations between AMO and the variables three months ahead are more intense than those of just one month later. For the 6-month lag time, most basins with significant correlations show the opposite direction to that observed with a 1-month lag time, for all variables analyzed. For example, the G3 basins start to show a negative correlation between GPP and AMO. In other words, while an increase in AMO indicates an increase in GPP in these basins in the following month, there is no significant influence on GPP three months later and, more surprisingly, it also indicates a reduction in GPP in these basins 6 months later. Spatially, the predominant north (positive) - south (negative) correlation pattern is evident (Fig. 3g,h). G4 basins show correlations predominantly ranging from − 0.35 to −0.44, while most G2 basins exhibit correlations between − 0.25 and − 0.34. In G3, only three basins have significant correlations, reaching up to −0.24. Conversely, G1 basins primarily display positive correlations, with values up to 0.24, although two basins in this group show negative correlations.

Regarding the AMM (Fig. 4), 90% of the basins showed significant negative correlations (Fig. 4n) with P at the 1st lag. especially in the central, southern and northeastern parts of Amazonia (part of G1 and G3) and

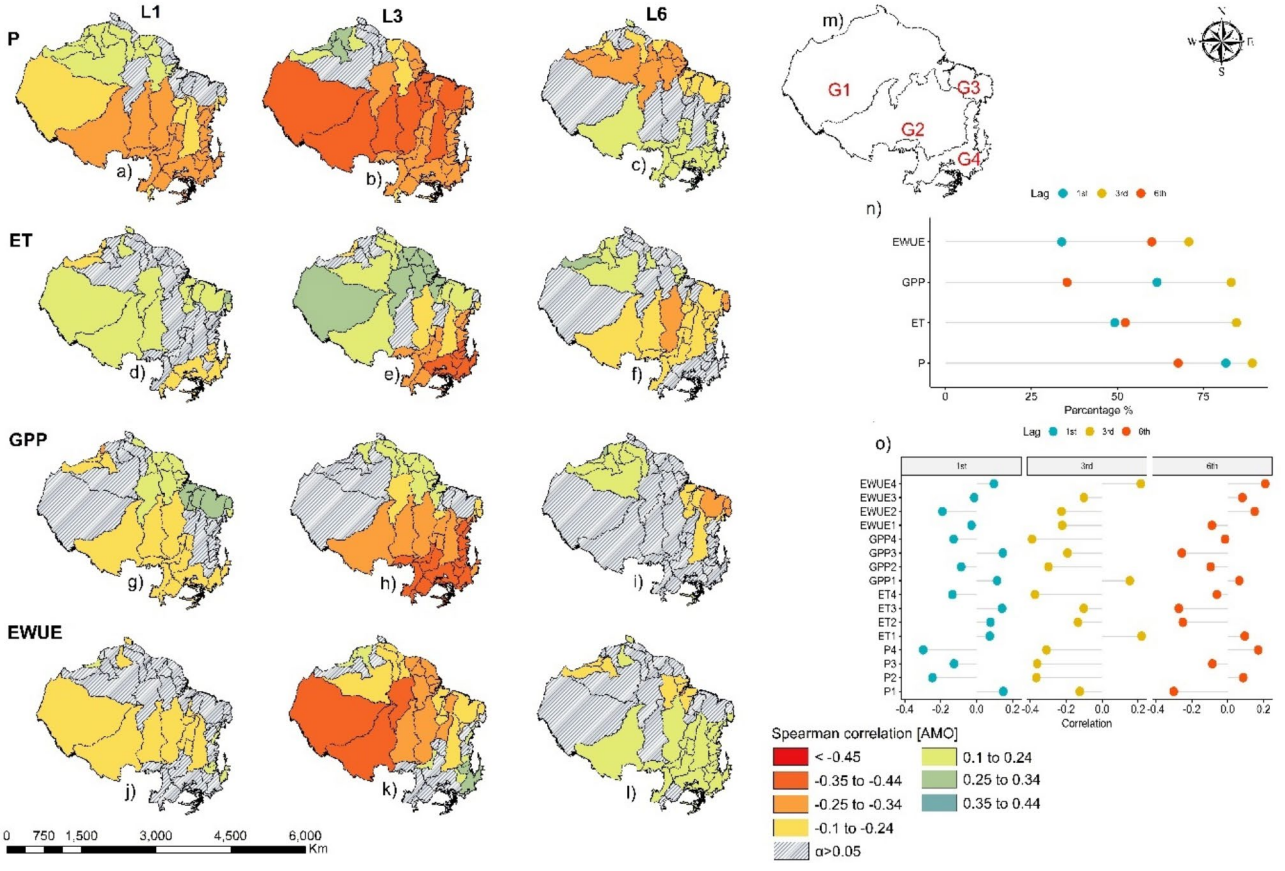

Fig. 3. Spearman correlation between AMO, precipitation and biophysical variables, for time lags of 1, 3 and 6 months (**a**–**l**), where columns are time lags and rows are biophysical variables [e.g., (**a**) is the correlation between P and AMO with a 1-month lag; (**b**) is the correlation between P and AMO with a 3-month lag]; (**m**) distribution of groups of watersheds; (**n**) is the percentage of watersheds with significant correlations for each variable in the three lags; and (**o**) Spearman correlation by cluster. The hitching identifies which case a particular watershed exhibits no statistical significance ($\alpha > 0.05$) in the correlation. The map was created with ArcGIS Desktop 10.8.1 (https://support.esri.com/en-us/patches-updates/2024/arcgis-desktop-10-8-1-general-component-updates-patch).

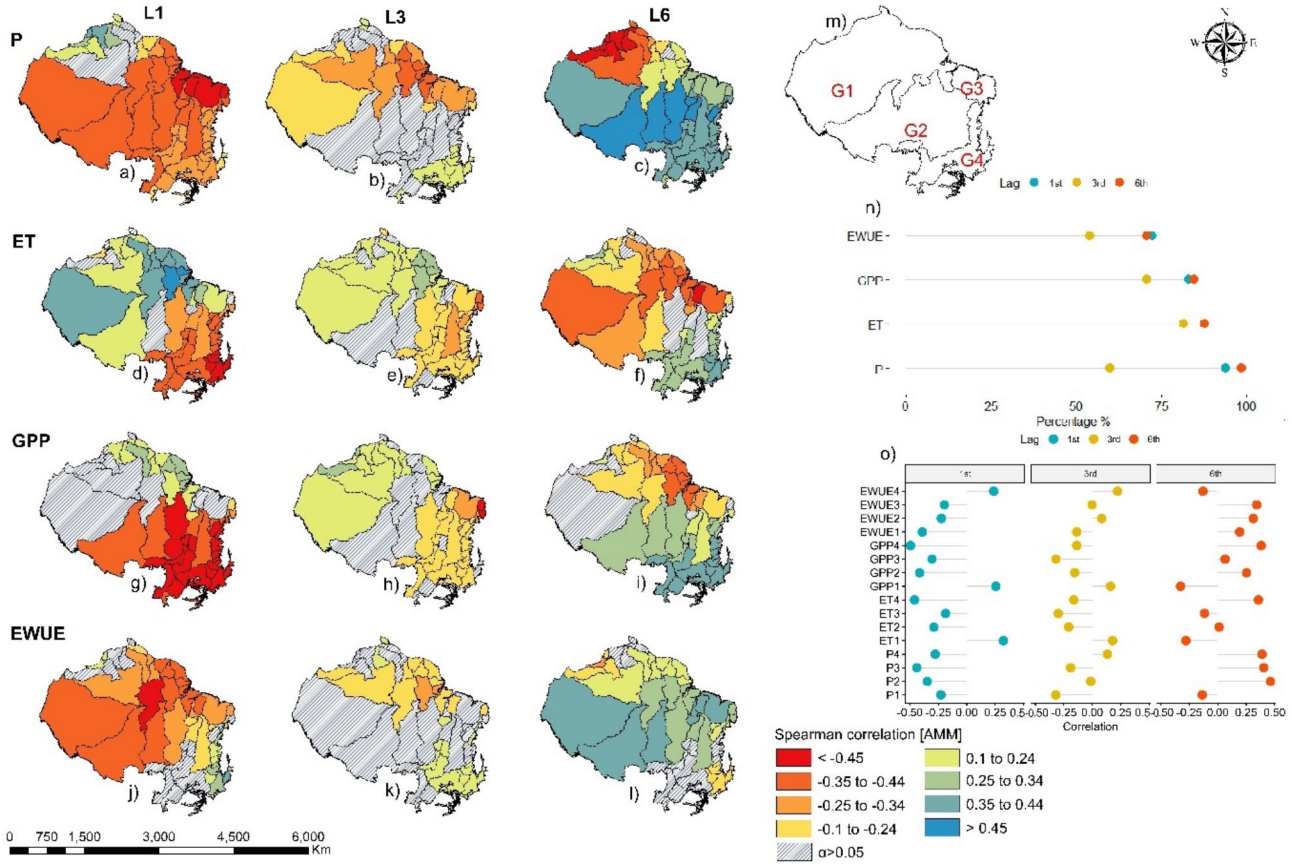

Fig. 4. Spearman correlation between AMM, precipitation and biophysical variables, for time lags of 1, 3 and 6 months (**a**–**l**), where columns are time lags and rows are biophysical variables [e.g., (**a**) is the correlation between P and AMO with a 1-month lag; (**b**) is the correlation between P and AMO with a 3-month lag]; (**m**) distribution of groups of watersheds; (**n**) is the percentage of watersheds with significant correlations for each variable in the three lags; and (**o**) Spearman correlation by cluster. The hitching identifies which case a particular watershed exhibits no statistical significance ($\alpha > 0.05$) in the correlation. The map was created with ArcGIS Desktop 10.8.1 (https://support.esri.com/en-us/patches-updates/2024/arcgis-desktop-10-8-1-general-component-updates-patch).

also in the Cerrado (G4), while 3% of the basins showed positive correlations in northern Amazonia (Fig. 4a). The percentage of significant basins drops to 60% in the 3rd lag-time (AMM-P, Fig. 4b), where most of the correlations were negative in G1 and G3, while G4 showed positive correlations.

At the 6th time lag 98% of the basins showed significant correlations between P and AMM, with a predominance of positive correlations in the south and northeast of the Amazon and also in the Cerrado, while in the north of the Amazon negative correlations were more evident. ET shows an opposite pattern to P with a lag of one month, where we obtained positive correlations in most of the G1 and G3 basins, this pattern is maintained in the 3rd lag-time for G1, but changes with a 6-month lag, where G1, G2 and G3 show negative correlations between ET and AMM and G4 shows positive correlations.

As for GPP at the 1st lag, 80% of the basins (Fig. 4n) showed negative correlations (<−0.45) in the south of the Amazon and in the Cerrado (G2 and G4). However, the basins in the north and northeast (G1 and G3, 3%) showed positive correlations of up to 0.34. With a lag of three months, the percentage of basins with significant correlations is reduced to 70%, where G1 predominates with positive correlations and G2 and G3 with negative correlations with AMM. The pattern is reversed in lag-6 (Fig. 4i), with G1 and G3 basins showing negative correlations (up to −0.44), while G2 and G4 showed positive correlations (0.24 to 0.44).

With a one-month lag between EWUE and AMM (Fig. 4j) we found predominantly (72%) negative correlations (<−0.45) in G1, G2 and G3, while G4 showed positive correlations between 0.24 and 0.34. At the 3rd lag, only 53% of the basins showed significant correlations, with the northern Amazon having predominantly negative correlations, while the southern Amazon and Cerrado (G2 and G4) had positive correlations (up to 0.24). With a six-month lag, positive correlations predominated in all groups, with G1, G2 and G3 showing the highest correlations (up to 0.44). In contrast, the basins of G4 and the northwest of G1 had negative correlations.

The ONI (Fig. 5) has no significant correlation with the analyzed variables (P, ET, GPP, and EWUE) for the following month in almost all of the 65 5th order river basins of the studied area. The exception was two basins in the western Amazon with a positive correlation between ONI and P. For a time, lag of three months, the

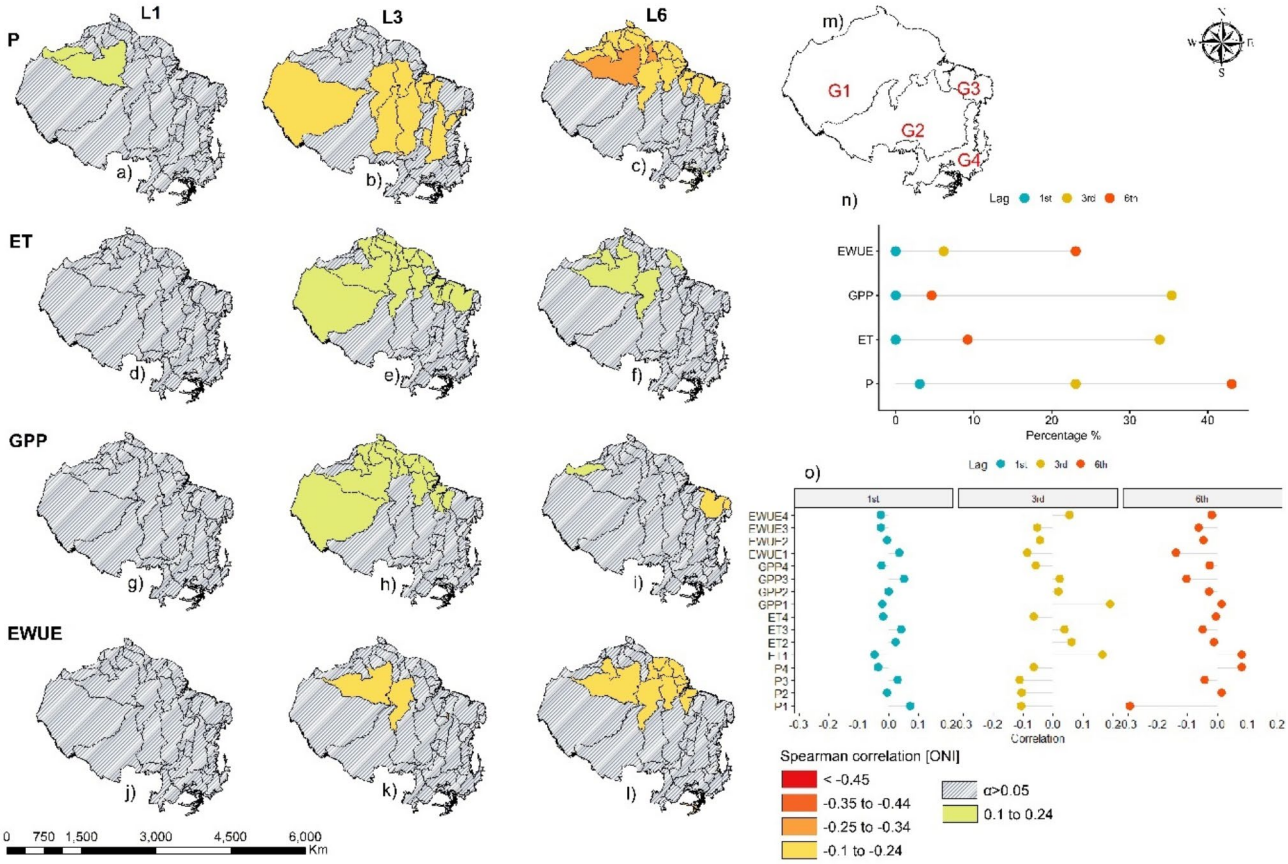

Fig. 5. Spearman correlation between ONI, precipitation and biophysical variables, for time lags of 1, 3 and 6 months (**a**–**l**), where columns are time lags and rows are biophysical variables [e.g., (**a**) is the correlation between P and AMO with a 1-month lag; (**b**) is the correlation between P and AMO with a 3-month lag]; (**m**) distribution of groups of watersheds; (**n**) is the percentage of watersheds with significant correlations for each variable in the three lags; and o) Spearman correlation by cluster. The hitching identifies which case a particular watershed exhibits no statistical significance ($\alpha > 0.05$) in the correlation. The map was created with ArcGIS Desktop 10.8.1 (https://support.esri.com/en-us/patches-updates/2024/arcgis-desktop-10-8-1-general-component-updates-patch).

influence of ONI in the region increases (Fig. 5n), with most basins of the northern Amazon (located in G1 and G3 groups) presenting positive correlation (0.1 to 0.24) between ONI and ET and GPP. This influence is reduced when a six-month time lag is applied. For P and EWUE, some basins in the middle Amazon show a negative correlation between ONI and P and EWUE for the three-month time lag, and this influence is amplified for more basins in the northern Amazon, mostly in G1, when a six months interval is considered.

Discussion

Around the world, research on the effects of teleconnections on biophysical variables is growing, such as[25,30–32]. However, research typically focuses on drought indices caused by ENSO and its impacts on precipitation or potential evapotranspiration that would lead to agricultural deficits. However, other teleconnections influence ecosystem services, hydroclimatic and energy regimes, and teleconnections usually interact with each other, causing even greater impacts. We analyzed four variables and six teleconnections in the largest biomes in South America and found that even within the same biome, there is significant spatial and temporal variability in biophysical variables (Fig. 1). For instance, the highest GPP is concentrated in the northwestern Amazon, coinciding with the region of highest rainfall (Fig. 1A,C). However, it is not a hotspot for evapotranspiration (ET) (Fig. 1B). The lower ET in this area, despite high GPP, results in elevated ecosystem water use efficiency (EWUE). The lower ET in this region is explained by the high cloudiness[28], making net radiation at the surface the main driver of evapotranspiration throughout the year[9].

In addition, ET in the Cerrado has strong stomatal control due to the high vapor pressure deficit (VPD), which is why the decrease in ET and GPP is less abrupt (Fig. 1E) in G4 compared to the other groups. These aspects were observed by[33] when he investigated the differences between evaporation, transpiration and GPP in the Amazon, Cerrado and Pantanal biomes[34]. Observed that, during the transition from the rainy to the dry season in a forest in southern Amazonia, the structural characteristics of the canopy played a more significant

role in controlling transpiration than direct water restrictions. This is due to the fact that the trees have stable water reserves even during the dry season.

Regions of lower EWUE in the south-east of the Amazon and in the Cerrado correspond mainly to the lower amount of biomass and high evapotranspiration characteristic of this region. This result agrees with[35] in a global description and[27] in their discussions of the Brazilian Amazon. The correlations observed between different groups of biophysical variables, such as between P2 and GPP4, or ET3 and EWUE2, indicate a possible spatial dependence, and it can be explained by hydrological memory in soil moisture[8,9,36,37], atmospheric moisture transport and precipitation recycling[9,34,35,37]. Furthermore, these processes help to clarify the temporal lags (Figs. 3, 4 and 5) between the onset of teleconnection cycles and the responses of biophysical variables. For example, during an El Niño event, until the event has fully matured (with the descending branch of the Walker cell covering the northern and northeastern South America)[38] with a vertical forcing inhibiting deep convection and thus decreasing precipitation in parts of G1, G2 and G3. This climatic condition was only identified with greater impact at a 3-month lag. Or in a negative AMM event, with the intensification of the northeast trade winds, which favors ET with a one-month lag.

Our results agree partially with[20], who analyzed the effects of teleconnections on global carbon fluxes. However, these authors do not mention the removal of autocorrelation in their time series. The authors also identified AMO as the main teleconnection modulating GPP in the southern portion of the Amazon and in the Cerrado. On the other hand, we disagree with the results where, according to[20], ONI assumes the role of the main modulator of GPP in the northern portion of the Amazon. In our results, AMM and AMO assume a leading role in the variability of the GPP in this region, since the AMM dominates the seasonal cycle of precipitation and evapotranspiration, while the AMO dominates the interdecadal balance, since both teleconnections modulate the transport of moisture and energy in the Amazon by displacing the ascending branch of the Hadley cell further north in the region. This displacement helps in the greater input of convective energy, added to the trade winds that drive ET3 (Fig. 6E), which explains the seasonal correlations between ET3 and AMO.

In addition, due to the tropospheric bridge between the Atlantic and Pacific oceans[39], the positive phase of AMO intensifies the Walker circulation[40], strengthening the Choco Jet in the coast of Colombia[41] and weakening the SACZ over the Brazilian Cerrado[42]. This explains the positive seasonal correlation between the EWUE and the AMO in the Cerrado during summer and spring (Fig. 6C).

In agreement with our results[25] founds that AMM modulates the LAI in the Amazon and Cerrado, which may explain its impact in GPP observed here. Physical explanations of teleconnections and their interactions with some hydroclimatic processes are discussed in depth by[24,37–40,43–45].

Regarding the time lag (Figs. 3, 4 and 5), most of the variables are inversely proportional to the main teleconnections studied, for example in the 1st lag-time (Fig. 3) between P and AMM or GPP and AMO, or even in the 3-month lag (Fig. 4) between AMO and EWUE or ONI and P. Our results partially agree with[46], where the authors evaluate the influence of ONI on hydrological processes in the eastern Amazon (equivalent to a part of G2 region in our study). The authors found negative and significant correlations between ONI and precipitation up to the 8th lag-time, and also positive correlations between this teleconnection and the reference evapotranspiration. Unlike[46], we did not find significant correlations with ONI and P in most basins/groups for various lag times, but we agree with the authors regarding ET. These findings make physical sense, wherein a positive (negative) El Niño (La Niña) ONI event, negative (positive) precipitation anomalies are expected in this region and, therefore, greater (less) solar radiation input to the surface, which leads to a positive correlation between ONI and ET (this also repeats for GPP), as seen in Figs. 4 and 5.

Corroborating our results[19], in a global analysis, found positive correlations between ENSO and GPP in the northern and western portions of the Amazon for the 3-month lag time and positive correlations in the same area for the 6-month lag time and negative correlations in the eastern portion of the Amazon with Cerrado, equivalent to our G3.

Although we do not present strong relationships with ENSO in our results, its influence on the Amazon and Cerrado is undeniable, especially in the last extreme events in the region, such as the droughts of 1998[47]; 2005[44]; 2010[48]; 2016[49]; 2022[50] or the floods of 2009 and 2012[40,51], respectively. However, these ENSO events were coupled with AMM, which confirms the importance of this teleconnection for the region, as well as strengthening the theory that the entire Earth system is connected (Fig. 6A), such as the tipping points[52]. Seasonally in the Amazon, this relationship between precipitation and ENSO is more visible (Fig. 6D), especially in summer (mature phase of the event) and spring (dry season), as observed by[16].

As in[25] we found a greater number of significant correlations (Figs. 3, 4 and 5) between AMM, AMO and biophysical variables than with ONI, for example. These teleconnections are known to affect the precipitation over South America due to their impacts on ITCZ meridional displacement and Hadley cell circulation[16,45]. An example is the positive correlations in the northern regions (G1 and G3) of the Amazon with AMM and ET in the 1st (Fig. 4e) lag-time, while in the southern portion of the Amazon and in the Cerrado (G2 and G4), these correlations are negative for these two variables. That is, these correlations occur because during the positive phase of AMM the ITCZ moves northward and moisture from the Atlantic Ocean is directed to northern Amazon, at same time that ascending branch of Hadley cell is more located over the north Amazon, favoring the convection. The moisture and convection are reduced in the southern Amazon during this phase of AMM[45], and with this there is a greater entry of radiation into the surface, which raises the temperature, triggering the ET-GPP biophysical feedback[53], which helps to explain the GPP2-AMM seasonal correlation observed in (Fig. 6B), with stronger correlation 6 months after the AMM maturation phase.

On the other hand, during the negative phase of AMM the ITCZ and ascending branch of Hadley cell moves more southward, and moisture from the Atlantic Ocean is direct to southern Amazon, where convection is favored, as well as favoring the occurrences of South Atlantic Convergence zone over the Cerrado region. The moisture and convection are reduced in the northern Amazon during this phase of AMM[45]. In addition

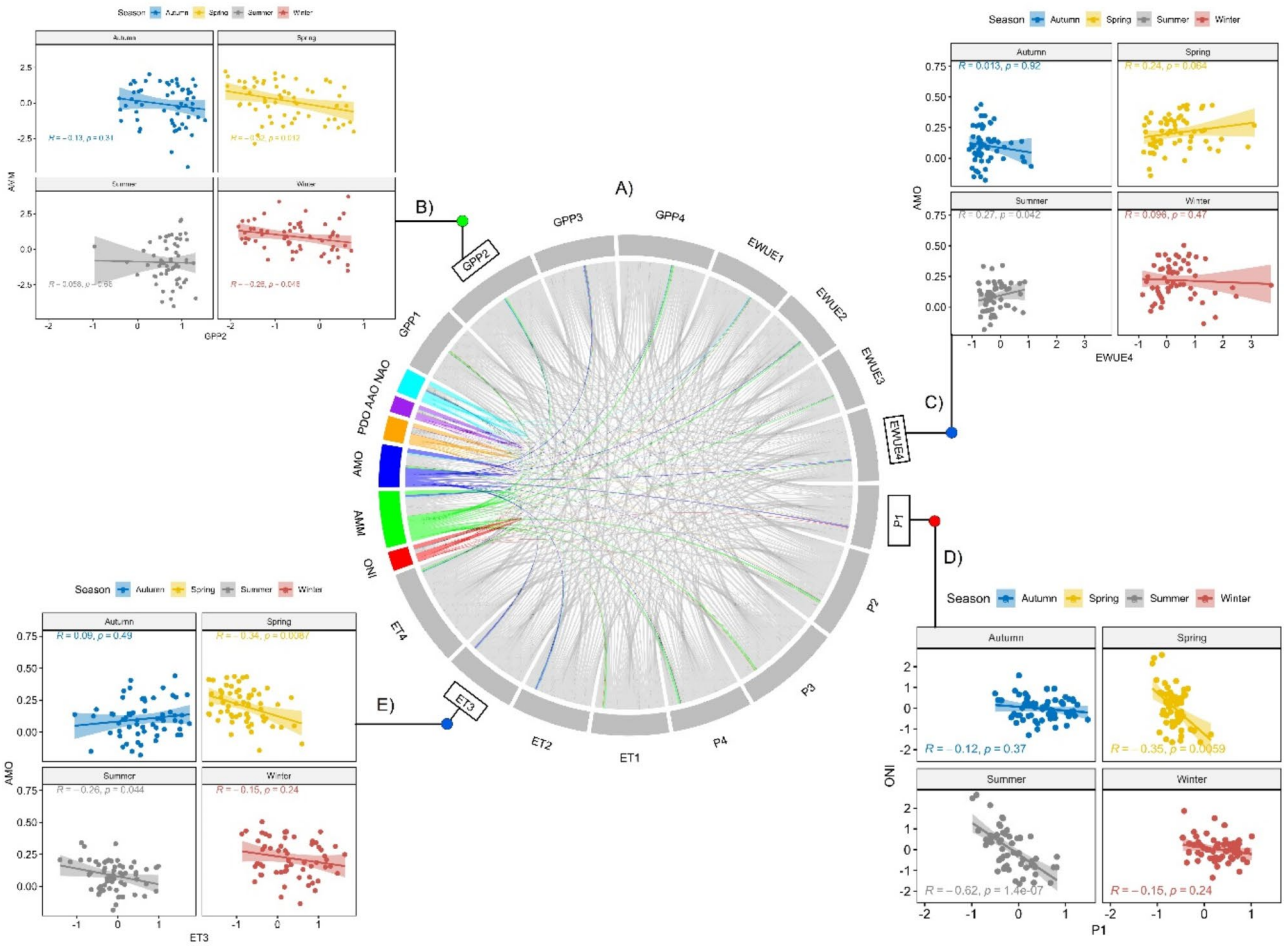

Fig. 6. Chord-Diagram (**A**) which shows the interconnections between the biophysical variables and the teleconnections for each group (i.e. P1, GPP2, ET3, EWUE4). The colors in gray show the correlations between the biophysical variables; Red shows the correlations with ONI; Light green are the correlations with AMM; Blue shows the correlations with AMO; Orange are the correlations with PDO; Purple are the correlations with AAO and Cyan are the correlations with NAO. (**B**) Expansion of the correlation between GPP2 and AMM; (**C** and **E**) are the correlations between AMO and EWUE4 and ET3, respectively; (**D**) are the correlations between P1 and ONI. The figure was created with R 4.3.1 (https://cran.r-project.org/).

to the impact of AMM on the precipitation, providing more water for evapotranspiration, the impact of this teleconnection on convection also affect the gas exchange and, consequently, carbon assimilation[7,27,53]. All these impacts trigger impacts on the interannual and seasonal cycle of biophysical variables analyzed here. However, it is also important to mention that the region G1 also include part of southern Amazon, and therefore, is affected in a more complex way at each stage of AMM.

Climate change is expected to amplify extreme events driven by teleconnections, impacting ecosystem services globally, although there is no consensus on the intensification of events like ENSO[54]. However, these future impacts can be observed, for instance, deforestation under CMIP6 scenarios could reduce biomass by up to 5.1% in the Amazon and 3.8% in the Congo[55], while global GPP may rise to 120,097 Pg C by 2100 under SSP5-8.5 scenarios[56]. Teleconnections already influencing ecosystems around the world, such as the AMM modulating the LAI (GPP driver) in regions such as northern Amazonia, subequatorial Africa and central Siberia[25].

Our results have limitations based on the products used that combine satellite estimates, modeling and in situ data (P, ET and GPP). Although these data are widely used around the world, there are uncertainties associated with the assimilation of in situ data with rainfall estimates in the infrared channel by CHIRPS or in the accuracy of the MODIS LAI product that supports ET estimates. Another limiting factor is the time series of biophysical data (20 years), which does not cover all the long-duration phases of teleconnections such as the AMO and PDO. Finally, we should be aware that the long-term terrestrial carbon fluxes simulated by PML-V2 still have uncertainties due to parameterization deficiencies and the scarcity of flux towers to improve the calibration of terrestrial ecosystem models. For this reason, we recommend using multiple data sources in future studies for P (e.g., IMERG-GPM, 3B43-TRMM, PERSIANN-CCS and CMORPH), ET (e.g., PML, GLEAM, SEBAL and METRIC) and GPP (e.g., MOD17A2H, VODCA2GPP, TRENDY-v7). In the supplementary material (Table

S1), we provide a set of P, ET, and GPP products used globally and provide a discussion of the accuracy of the products used.

The overview of dominant global and regional teleconnections presented here offers valuable guidance for selecting the most relevant teleconnection patterns when studying local and regional ecosystem services, particularly in two of the world's most critical biodiversity hotspots: The Amazon and the Cerrado. This information is also useful for stochastic forecasting in carbon sink dynamics (such as reforestation efforts) and mitigating extreme weather events' impacts on agricultural activities.

For instance, a 6-month lag in the AMO can indicate potential evapotranspiration (ET) deficits in southern Amazon and Cerrado regions—key areas for Brazil's agricultural production. Similarly, a 3-month ONI lag can signal decreased precipitation in the south of Amazon. The AMM, with the same 3-month lag, also tends to enhance carbon assimilation in the northern Amazon, providing critical insights for managing carbon sinks and ecosystem services in response to climate variability.

Data and methods

Study area

The study area (Fig. 7) comprises the Amazon and Cerrado biomes. The Amazon encompasses 9 countries, holds the largest territorial extension (~7.5 million km²) of tropical forest in the world, and is home to more than 40 million inhabitants, with emphasis on 385 indigenous peoples[57]. Its hydroclimatic characteristics vary spatially, with average annual precipitation of 2,200 mm.year^{-1}[58], of which around 20% is regionally recycled by evapotranspiration (varying between 15% and 25% in different Amazonian subregions and seasons of the

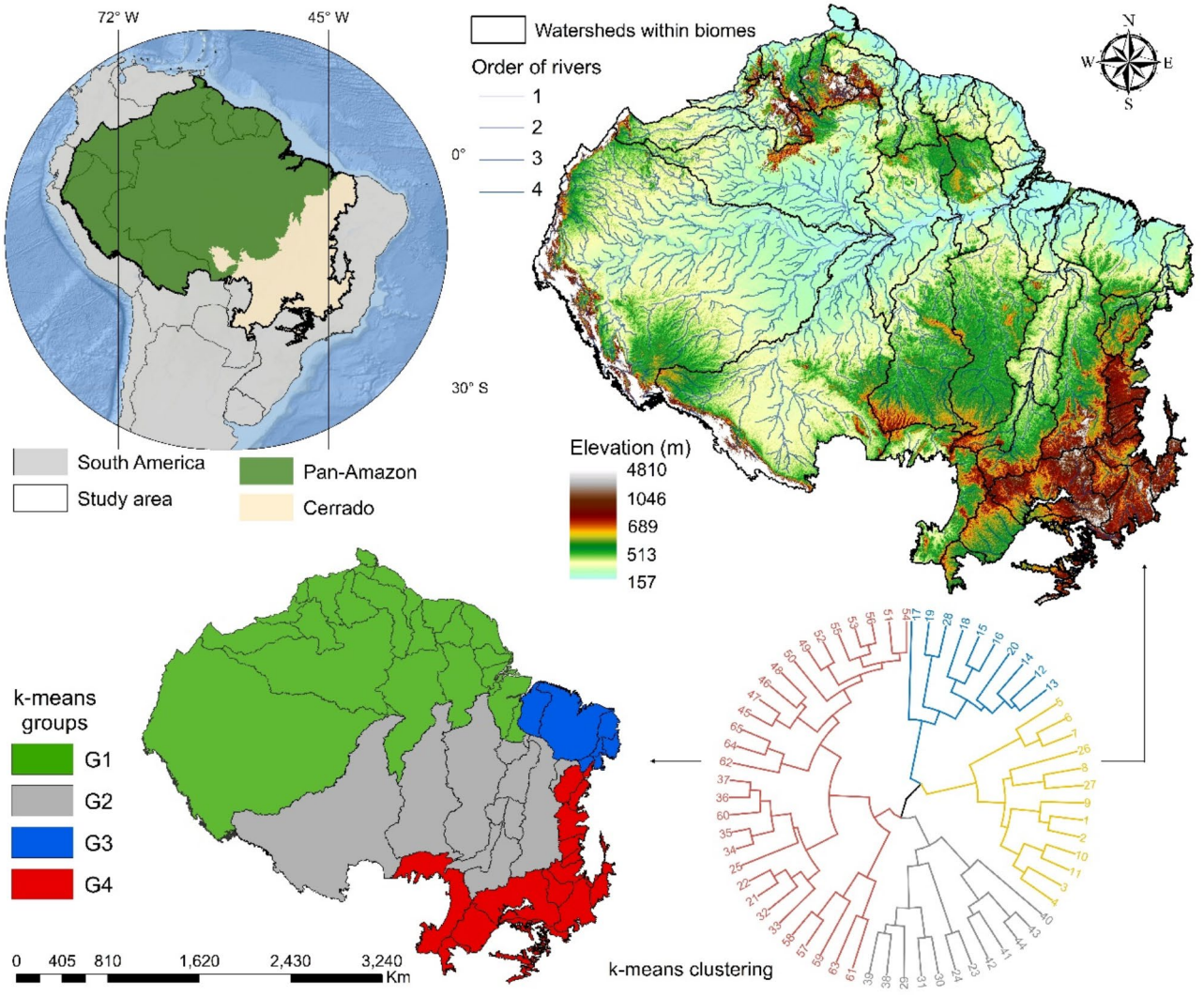

Fig. 7. Location of the Amazon and Cerrado biomes; elevation and division of these biomes into 5th order hydrographic basins; and grouping of these watersheds into four groups of same GPP. The map was created with ArcGIS Desktop 10.8.1 (https://support.esri.com/en-us/patches-updates/2024/arcgis-desktop-10-8-1-general-component-updates-patch).

Region	Teleconnection	Description	Reference
Pacific	ONI	Three month running mean of NOAA ERSST.V5 SST anomalies in the Niño 3.4 region (5 N-5 S, 120–170 W).	67
	PDO	1st Empirical Orthogonal Function of North Pacific SST and Sea Level Pressure anomalies (100°E–100°W, 20–65°N).	68
Atlantic	AMM	2nd principal component of tropical Atlantic SST anomalies and the zonal and meridional components of wind (70°W–20°E, 30°S–30°N).	69
	AMO	Average SST anomalies for the North Atlantic (80°W–0°E, 0–60°N).	70
Atmosphere	AAO	1st leading mode from the EOF analysis of monthly mean height anomalies at 700-hPa poleward of 20°S.	71,72
	NAO	1st principal component of sea level pressure anomalies over the North Atlantic (90°W–20°E, 20–80°N)	73

Table 1. Detailed information about the analyzed indexes of climate variability (teleconnections) analyzed.

year), and the rest of evapotranspiration and oceanic moisture are transported downwind to the La Plata Basin, mainly[37]. Moreover, the hydroclimatic characteristics of this biome, located in the Earth's largest watershed, is responsible for the world's largest streamflow: $206 \times 10\ m^3.s^{-1}$[59,60].

The Cerrado biome (Brazilian tropical savannah) is a biodiversity hotspot, with the most diverse flora of any savannah in the world[61]. The biome covers approximately 2 million km^2, which corresponds to 24% of the Brazilian territory[62], and covers an area of water recharge for important aquifers and rivers in South America and for the generation of hydroelectric energy in Brazil[63]. The predominant climate is tropical savannah, characterized by two well-defined seasons (monsoon regime), and average annual precipitation of ~1480 mm. $year^{-1}$[64,65]. In the bordering regions, the climate transitions to a hot semi-arid condition (Northeast), a tropical monsoon climate (West), and a temperate climate (South)[66].

Teleconnections

We analyzed six globally important climate variabilities (ENSO, PDO, AMO, AMM, AAO and NAO), as shown in Table 1. Monthly data for the 6 teleconnections indices are obtained from the National Oceanic and Atmospheric Administration (NOAA).

It is also important to mention that the periodicity of AMO (50–88 years[74]) and PDO (50–70 years[68]) are longer than the time series used in this study (20 years). However, at same time that the indexes about these two climatic variabilities are calculated at monthly time scale[68,70], these variables also have quasi-oscilations on shorter time scales[75].

Gross primary production (GPP)

We used monthly GPP data between 2001 and 2020 from the Penman-Monteith-Leuning V2 model (PML-V2[29,76]). The PML-V2 product uses the Penman-Monteith evapotranspiration equation modified by[77], changing the surface conductance formulation considering soil and canopy water losses and using a biophysical canopy conductance model that combines GPP with canopy transpiration[76]. The version 2 is improved by incorporating the vapor pressure deficit constraint into the GPP, which is then used to constrain canopy conductance and transpiration.

The product has high accuracy compared with global ground observations, although it can underestimate GPP in rainforests[29]. Furthermore, the PML-V2 GPP can be considered more improved than the MOD17 GPP product because the MODIS ET and GPP algorithms are not coupled, that is, one product is independent of the other, when in fact the GPP is strongly dependent on stomatal conductance[29,76]. PLM-V2 products are calibrated and validated using flow tower data from FLUXNET2015, and specific results for a tower in the Amazon reveal superior performance (RMSE = 1.17) of PLM compared to GPP of MOD17A2H (RMSE = 4.34)[29]. Furthermore, global comparisons[78–81] demonstrate the good performance of PML.

Evapotranspiration (ET)

Evapotranspiration data were obtained using the MOD16A2 product, based on the Penman-Monteith evapotranspiration equation[82]. This product integrates land cover (MOD12Q1), albedo (MCD43), LAI, photosynthetically active radiation fraction (MOD15A2), and meteorological data reanalysis[83] to obtain potential and actual evapotranspiration with 500 m resolution every 8 days. MOD16A2 evapotranspiration data is available at Google Earth Engine and was integrated monthly from 2001 to 2020 according to GPP data. This evapotranspiration product is widely used and has already been validated and tested for the Amazon[84,85] and Cerrado[86,87] in addition to the transition between biomes[88]. Catchment-mean ET values from this product is strongly correlated with ET from the catchment-balance for the Amazon[89].

Monthly water use efficiency (WUE) was calculated as the ratio of GPP and ET and represents the amount of carbon gained by water unit used[11]. It is commonly called Ecosystem Water Use Efficiency (EWUE) due to the change in vegetation's photosynthesis rate in relation to the use of water[90].

Precipitation (P)

We used the Climate Hazards Group InfraRed Precipitation with Station data (CHIRPS v2.0)[91]. The algorithm combines weather station data and incorporates satellite information to represent sparsely measured locations, and daily, pentad, and monthly precipitation estimates of 0.05° infrared estimates of Cold Cloud Duration from 1981 to present. The monthly average from 2001 to 2020 with 0.05° of spatial resolution was obtained from Google Earth Engine. The product was developed for trend analysis and seasonal drought monitoring and had

presented a great performance in representing monthly precipitation throughout the Brazilian Amazon and parts of Cerrado[92–95]. We leave a detailed review on all the products used and their accuracy for our study area in the supplementary material.

Statistical analysis

Time lag and clustering.

The first step in processing the data was to remove autocorrelation from the time series, especially from the teleconnections. According to[96], as the teleconnections interact with each other, their signal is usually loaded with biases that can often lead researchers to unexpected results. We therefore used the differentiation method to remove autocorrelation from our time series according to Eqs. 1 and 2. This procedure was carried out using the Pandas library[97] on Google Colab.

$$Y_t = (1 - B)^d (1 - b = B^s)^D X_t \tag{1}$$

being d the order of the first differencing component, s is the period of the seasonal component, D is the order of the seasonal component, and B is the lag operator defined by:

$$BX_t = X_{t-1} \tag{2}$$

The values of (d, D) can be chosen in an interactive process, or as a function of Autocorrelation and Partial Autocorrelation (ACF, PACF). s is 12 for monthly data with annual seasonality and 0 when there is no seasonality.

The standardized anomaly (Eq. 3) of the biophysical variables was also calculated so that correlations could be made in time lag with the anomalies of the teleconnections without autocorrelation. After all the data treatments on the variables (teleconnections, precipitation and biophysical variables), Spearman's correlation was carried out with a time lag of 1, 3 and 6 months between teleconnections, precipitation and biophysical variables for each basin and for each cluster. These time lags were selected because they obtained the best correlations with statistical significance. In addition, these lags correspond to the average time of development, maturation and dissipation of some teleconnections, such as ENSO and AMM (with the exception of AMO and PDO). These aspects have been previously discussed by[98–104]

$$SA = \frac{X_t - \bar{X}}{\sigma} \tag{3}$$

being SA the standardized anomaly, X_t is the value of the biophysical variable for a time t, here it is the monthly value of the biophysical variable, P for example. $\bar{X}$ is the average of the biophysical variable for the study period, that is 20 years, and σ is the standard deviation of the biophysical variable for the same study period.

Due to the number of river basins to be studied, we used K-means clustering to group the basins with the same GPP pattern (Fig. 7) and thus reduced the 59 basins to 4 groups (G1 = 26, G2 = 12, G3 = 8, G4 = 19) of basins. Finally, we performed correlation products (Spearman, with significance level $\alpha = 0.05$) of the groups of biophysical variables with each other and between the teleconnections; these processes were carried out in R using the factoextra and corrplot packages[105], respectively. From this point onwards (display of correlation results, relative importance and Lag-time) we call GPP1, GPP2, GPP3 and GPP4 the GPP of groups 1, 2, 3 and 4. The same for ET, P and EWUE.

Finally, we applied the Kruskal-Wallis non-parametric statistical tests for k samples, the Steel-Dwass-Critchlow-Fligner paired multiple comparisons test and the Kolmogorov-Smirnov test to confirm that all the data series (biophysical, precipitation and teleconnections) were properly transformed into series without autocorrelation and that the K-means groupings really did form consistent and independent groups. In addition, we constructed ACF graphs for time lags of up to 6 months for the teleconnections and groupings of the biophysical variables and precipitation. The Kruskal-Wallis test allows us to identify whether the samples come from the same population, while the Kolmogorov-Smirnov test indicates whether the distribution of the two samples is the same, while the Steel-Dwass-Critchlow-Fligner test shows whether there are significant differences between the time series. All the statistics were carried out at a significance level of 0.05 and the graphical and tabular results can be found in the supplementary material.

Regression analysis and relative importance.

To assess the influence of ocean-atmosphere teleconnections on biophysical variables (P, ET, GPP, and EWUE), we first establish a relationship between these biophysical variables (Y) and the ocean-atmosphere indices (X) from Table 1 using a regression model according to[106]. Here, X represents each index within the set S, denoted as X_j, $J \in S$:

$$Y = \alpha_0 + \sum\nolimits_{j \in S} \alpha_j X_j \tag{4}$$

being α_0 and α_j unknown intercept and regression coefficients. When the coefficients are estimated ($\widehat{\alpha}_0$ and $\widehat{\alpha}_j$), the fitted variable $\widehat{Y}$ can be written as:

$$\widehat{Y} = \widehat{\alpha}_0 + \sum\nolimits_{j \in S} \widehat{\alpha}_j X_j \tag{5}$$

The coefficient of determination, R^2, measures the proportion of variation in Y that is explained by the variables X in the regression model, which is usually used to evaluate the goodness of fit of the model. It is written as:

$$R^2(S) = \frac{\sum_{i-1}^{n} \left(\widehat{Y}_i - \bar{Y}\right)^2}{\sum_{i=1}^{n} \left(Y_i - \bar{Y}\right)^2} \tag{6}$$

To identify the most significant variables for the Y variable, relative importance analysis is applied, i.e., which teleconnection is most important for the biophysical variables. This approach involves decomposing the R^2 to assess the individual contributions of each independent variable to the total R^2. In a model with independent variables in the data set S, the explanation of the variance of the dependent variable is R^2(S). By adding independent variable X_k to the regression model for set S, the R^2 of X_k can be written as:

$$R^2\left(\{X_k\}|S\right) = R^2\left(\{X_k\}|\cup S\right) - R^2\left(S\right) \tag{7}$$

Considering the effects of the orderings of the correlated variables that entered the model, the R^2 of X_k in order r (denoted as set S^r) can be written as:

$$seqR^2\left(\{X_k\}|S^r\right) = R^2\left(\{X_k\}|\cup\ S^r\right) - R^2\left(S^r\right) \tag{8}$$

Based on Eq. (9), the Lindeman Merenda and Gold (LMG) method[107] was used; this LMG method is an average of all possible orderings of correlated variables.

$$LMGX_k = \frac{1}{p!}\sum\nolimits_{rpermutation} seqR^2\left(\{X_k\}|S^r\right) \tag{9}$$

being p the number of independent variables X, and r denotes r-permutation, i.e., $r = 1, 2, \ldots, p$.

In this way we know which independent variables (teleconnections) have the greatest influence on the biophysical variables for each group of river basins. This approach has been used in applications around the world, e.g.[23], investigated the impacts of teleconnections on hydrometeorological variables in five river basins in Southeast Asia[27]; used the random forest machine learning algorithm to classify the most important variables in the carbon sink process in secondary forests in the Amazon.

Data availability

The original data used in this study are all publicly available from their sources: P (https://developers.google.com/earth-engine/datasets/catalog/UCSB-CHG_CHIRPS_DAILY); GPP (https://developers.google.com/earth-engine/datasets/catalog/CAS_IGSNRR_PML_V2_v018) and ET (https://developers.google.com/earth-engine/datasets/catalog/MODIS_061_MOD16A2) for Teleconnection (https://psl.noaa.gov/data/climateindices/list/). In addition, the raw data used in this study by watershed is available at: (https://doi.org/10.6084/m9.figshare.28009082).

Code availability

The computer codes that support the analysis carried out in this article (relative importance) are available on request from the corresponding author. The codes for extracting the biophysical data (GPP, ET and P), as well as the code for extracting the autocorrelation and running the lag-time correlations can be found at (https://github.com/oliveiraserrao), via the [Lag-Time] and [Biophysical-data] repositories.

Received: 27 September 2024; Accepted: 1 January 2025
Published online: 09 January 2025

References

1. Le Quéré, C. et al. Global carbon budget 2018. *Earth Syst. Sci. Data* **10**, 2141–2194 (2018).
2. Beer, C. et al. Terrestrial gross carbon dioxide uptake: Global distribution and covariation with climate. *Science (80-)* **329**, 834–838 (2010).
3. Xu, S., Li, J. & Zhang, T. Effects of drought on ecosystem evapotranspiration and gross primary productivity in the Haihe River Basin. *Phys. Chem. Earth Parts A/B/C* 103619 https://doi.org/10.1016/j.pce.2024.103619 (2024).
4. Wohlfahrt, G. & Gu, L. The many meanings of gross photosynthesis and their implication for photosynthesis research from leaf to globe. *Plant Cell Environ.* **38**, 2500–2507 (2015).
5. Liao, Z., Zhou, B., Zhu, J., Jia, H. & Fei, X. A critical review of methods, principles and progress for estimating the gross primary productivity of terrestrial ecosystems. *Front. Environ. Sci.* **11** (2023).
6. Mo, L. et al. Integrated global assessment of the natural forest carbon potential. *Nature* **624**, 92–101 (2023).
7. Lee, D., Kim, J. S., Park, S. W. & Kug, J. S. An abrupt shift in gross primary productivity over Eastern China-Mongolia and its inter-model diversity in land surface models. *Sci. Rep.* **13**, 22971 (2023).
8. Zanin, P. R. Soil water uptake by amazonian trees and simulation of impacts on energy fluxes and soil moisture dynamics at the LBA flux towers. *Rev. Bras. Meteorol.* **36**, 441–454 (2021).
9. Zanin, P. R., Pareja-Quispe, D. & Espinoza, J. C. Evapotranspiration in the Amazon basin: Couplings, hydrological memory and water feedback. *Agric. Meteorol.* **352**, 110040 (2024).
10. Cowan, I. R. Regulation of water use in relation to carbon gain in higher plants. in *Physiological Plant Ecology II* 589–613 (Springer, Berlin, 1982). https://doi.org/10.1007/978-3-642-68150-9_18
11. Naeem, S. et al. Recent change in ecosystem water use efficiency in China mainly dominated by vegetation greening and increased CO2. *Remote Sens. Environ.* **298**, 113811 (2023).
12. Sun, S. et al. Spatio-temporal variations in water use efficiency and its drivers in China over the last three decades. *Ecol. Indic.* **94**, 292–304 (2018).
13. Kruid, S. et al. Beyond deforestation: Carbon emissions from land grabbing and forest degradation in the Brazilian Amazon. *Front. Glob Chang.* **4** (2021).

14. Sylvester, J. M. et al. Analysis of food system drivers of deforestation highlights foreign direct investments and urbanization as threats to tropical forests. *Sci. Rep.* **14**, 15179 (2024).
15. Yuan, M. et al. Global response of terrestrial gross primary productivity to climate extremes. *Sci. Total Environ.* **750**, 142337 (2021).
16. Reboita, M. S. et al. Impacts of teleconnection patterns on South America climate. *Ann. N Y Acad. Sci.* **1504**, 116–153 (2021).
17. Liu, Z. & Alexander, M. Atmospheric bridge, oceanic tunnel, and global climatic teleconnections. *Rev. Geophys.* **45** (2007).
18. Kucharski, F., Kang, I. S., Straus, D. & King, M. P. Teleconnections in the atmosphere and oceans. *Bull. Am. Meteorol. Soc.* **91**, 381–383 (2010).
19. Zhang, Y., Dannenberg, M. P., Hwang, T. & Song, C. El Niño-Southern Oscillation-induced variability of terrestrial gross primary production during the satellite era. *J. Geophys. Res. Biogeosciences.* **124**, 2419–2431 (2019).
20. Zhu, Z. et al. The effects of teleconnections on carbon fluxes of global terrestrial ecosystems. *Geophys. Res. Lett.* **44**, 3209–3218 (2017).
21. Woodward, F., Lomas, M. & Quaife, T. Global responses of terrestrial productivity to contemporary climatic oscillations. *Philos. Trans. R. Soc. B Biol. Sci.* **363**, 2779–2785 (2008).
22. Ying, K., Peng, J., Dan, L. & Zheng, X. Ocean—atmosphere teleconnections play a key role in the Interannual variability of seasonal gross primary production in China. *Adv. Atmos. Sci.* **39**, 1329–1342 (2022).
23. He, Q. et al. Three-dimensional Budyko framework incorporating terrestrial water storage: Unraveling water-energy dynamics, vegetation, and ocean-atmosphere interactions. *Sci. Total Environ.* **904**, 166380 (2023).
24. Wharton, S., Chasmer, l., Falk, M. & Paw U, K. T. Strong links between teleconnections and ecosystem exchange found at a pacific northwest old-growth forest from flux tower and MODIS EVI data. *Glob. Change Biol.* **15**, 2187–2205 (2009).
25. Dahlin, K. M. & Ault, T. R. Global linkages between teleconnection patterns and the terrestrial biosphere. *Int. J. Appl. Earth Obs. Geoinf.* **69**, 56–63 (2018).
26. Kayano, M. T., Andreoli, R. V. & de Ferreira, R. A. Relations between ENSO and the South Atlantic SST modes and their effects on the south American rainfall. *Int. J. Climatol.* **33**, 2008–2023 (2013).
27. Heinrich, V. H. A. et al. Large carbon sink potential of secondary forests in the Brazilian Amazon to mitigate climate change. *Nat. Commun.* **12**, 1785 (2021).
28. Hu, Y., Wei, F., Fu, B., Zhang, W. & Sun, C. Ecosystems in China have become more sensitive to changes in water demand since 2001. *Commun. Earth Environ.* **4**, 444 (2023).
29. Zhang, Y. et al. Coupled estimation of 500 m and 8-day resolution global evapotranspiration and gross primary production in 2002–2017. *Remote Sens. Environ.* **222**, 165–182 (2019).
30. Bastos, A. et al. European land CO_2 sink influenced by NAO and East-Atlantic pattern coupling. *Nat. Commun.* **7**, 10315 (2016).
31. Fancourt, M. et al. Background climate conditions regulated the photosynthetic response of Amazon forests to the 2015/2016 El Nino-Southern Oscillation event. *Commun. Earth Environ.* **3**, 209 (2022).
32. Wu, M. et al. Regional responses of vegetation productivity to the two phases of ENSO. *Geophys. Res. Lett.* **51** (2024).
33. D'Acunha, B. et al. Changes in evapotranspiration, transpiration and evaporation across natural and managed landscapes in the Amazon, Cerrado and Pantanal biomes. *Agric. Meteorol.* **346**, 109875 (2024).
34. Vourlitis, G. L. et al. Energy balance and canopy conductance of a tropical semi-deciduous forest of the southern Amazon Basin. *Water Resour. Res.* **44** (2008).
35. Shevliakova, E. et al. Carbon cycling under 300 years of land use change: importance of the secondary vegetation sink. *Glob. Biogeochem. Cycles* **23** (2009).
36. Cavalcante, R. B. L. et al. Terrestrial water storage and Pacific SST affect the monthly water balance of Itacaiúnas River Basin (Eastern Amazonia). *Int. J. Climatol.* **40**, 3021–3035 (2020).
37. Zanin, P. R., Satyamurty, P., Inter-seasonal and inter-basins hydrological coupling in South America. *J. Hydrometeorol.* https://doi.org/10.1175/JHM-D-20-0080.1 (2021).
38. Tedeschi, R. G. & Sampaio, G. Influences of different intensities of El Niño–Southern Oscillation on South American precipitation. *Int. J. Climatol.* **42**, 7987–8007 (2022).
39. Wang, C. An overlooked feature of tropical climate: Inter-pacific-atlantic variability. *Geophys. Res. Lett.* **33**, 1–5 (2006).
40. Barichivich, J. et al. Recent intensification of Amazon flooding extremes driven by strengthened Walker circulation. *Sci. Adv.* **4** (2018).
41. Cerón, W. L. et al. Pacific and atlantic multidecadal variability relations with the choco and caribbean low-level jets during the 1900–2015 period. *Atmosphere (Basel)* **12** (2021).
42. Chiessi, C. M., Mulitza, S., Pätzold, J., Wefer, G. & Marengo, J. A. Possible impact of the Atlantic multidecadal oscillation on the South American summer monsoon. *Geophys. Res. Lett.* **36**, 1–5 (2009).
43. Dominguez, F. et al. Amazonian moisture recycling revisited using WRF with Water Vapor Tracers. *J. Geophys. Res. Atmos.* **127** (2022).
44. Marengo, J. et al. The drought of Amazonia in 2005. *J. Clim.* **21**, 495–516 (2008).
45. Zanin, P. R. & Satyamurty, P. Hydrological processes interconnecting the two largest watersheds of South America from multi-decadal to inter-annual time scales: A critical review. *Int. J. Climatol.* **40**, 4006–4038 (2020).
46. Cavalcante, R. B. L., Pontes, P. R. M., Souza-Filho, P. W. M. & Souza, E. B. Opposite effects of climate and land use changes on the annual water balance in the Amazon arc of deforestation. *Water Resour. Res.* **55**, 3092–3106 (2019).
47. Tomasella, J. et al. The droughts of 1996–1997 and 2004–2005 in Amazonia: Hydrological response in the river main-stem. *Hydrol. Process.* **25**, 1228–1242 (2011).
48. Lewis, S. L., Brando, P. M., Phillips, O. L., van der Heijden, G. M. F. & Nepstad, D. The 2010 Amazon drought. *Science (80-)* **331**, 554–554 (2011).
49. Jiménez-Muñoz, J. C. et al. Record-breaking warming and extreme drought in the Amazon rainforest during the course of El Niño 2015–2016. *Sci. Rep.* **6**, 33130 (2016).
50. Espinoza, J. C. et al. The new record of drought and warmth in the Amazon in 2023 related to regional and global climatic features. *Sci. Rep.* **14**, 8107 (2024).
51. Chen, J. L., Wilson, C. R. & Tapley, B. D. The 2009 exceptional Amazon flood and interannual terrestrial water storage change observed by GRACE. *Water Resour. Res.* **46** (2010).
52. Liu, T. et al. Teleconnections among tipping elements in the earth system. *Nat. Clim. Chang.* **13**, 67–74 (2023).
53. Ritter, F., Berkelhammer, M. & Garcia, C. Distinct response of gross primary productivity in five terrestrial biomes to precipitation variability. *Commun. Earth Environ.* **1**, 34 (2020).
54. Tedeschi, R. G. & Collins, M. The influence of ENSO on South American precipitation: Simulation and projection in CMIP5 models. *Int. J. Climatol.* **37**, 3319–3339 (2017).
55. Li, Y. et al. Deforestation-induced climate change reduces carbon storage in remaining tropical forests. *Nat. Commun.* **13**, 1964 (2022).
56. Lu, Q., Liu, H., Wei, L., Zhong, Y. & Zhou, Z. Global prediction of gross primary productivity under future climate change. *Sci. Total Environ.* **912**, 169239 (2024).
57. OTCA (Amazon Cooperation Treaty Organization). *El Cambio Climático en la Región Amazónica - Acciones de la Otca*. http://otca.org/wp-content/uploads/2020/07/El-Cambio-Climático-en-la-Región-Amazónica-Acciones-de-la-OTCA.pdf (2020).

58. Espinoza Villar, J. C. et al. Spatio-temporal rainfall variability in the Amazon basin countries (Brazil, Peru, Bolivia, Colombia, and Ecuador). *Int. J. Climatol.* **29**, 1574–1594 (2009).
59. Callède, J. et al. Les apports en eau de l'Amazone à l'Océan Atlantique. *Rev. Des. Sci. L'eau.* **23**, 247–273 (2010).
60. Fassoni-Andrade, A. C. et al. Amazon Hydrology from Space: scientific advances and Future challenges. *Rev. Geophys.* **59**, (2021).
61. Lambers, H., de Britto Costa, P., Oliveira, R. S. & Silveira, F. A. O. towards more sustainable cropping systems: Lessons from native Cerrado species. *Theor. Exp. Plant Physiol.* **32**, 175–194 (2020).
62. EMBRAPA (Brazilian agricultural research company). Cerrado: Ecologia e Flora (2008).
63. da Amorim, J. S. et al. Quantifying the climate change-driven impacts on the hydrology of a data-scarce watershed located in the Brazilian Tropical Savanna. *Hydrol. Process.* **36** (2022).
64. Alvares, C. A., Stape, J. L., Sentelhas, P. C., de Moraes Gonçalves, J. L. & Sparovek, G. Köppen's climate classification map for Brazil. *Meteorol. Z.* **22**, 711–728 (2013).
65. Campos, J. D. O. & Chaves, H. M. L. Tendências e Variabilidades nas Séries Históricas de Precipitação Mensal e Anual no Bioma Cerrado no Período 1977–2010. *Rev. Bras. Meteorol.* **35**, 157–169 (2020).
66. Althoff, D., Rodrigues, L. N. & da Silva, D. D. Assessment of water availability vulnerability in the Cerrado. *Appl. Water Sci.* **11**, 176 (2021).
67. Huang, B. et al. Extended reconstructed sea surface temperature, version 5 (ERSSTv5): Upgrades, validations, and intercomparisons. *J. Clim.* **30**, 8179–8205 (2017).
68. Mantua, N. J., Hare, S. R., Zhang, Y., Wallace, J. M. & Francis, R. C. A pacific interdecadal climate oscillation with impacts on salmon production. *Bull. Am. Meteorol. Soc.* **78**, 1069–1079 (1997).
69. Chiang, J. C. H. & Vimont, D. J. Analogous Pacific and Atlantic meridional modes of tropical atmosphere–ocean variability*. *J. Clim.* **17**, 4143–4158 (2004).
70. Enfield, D. B., Mestas-Nuñez, A. M. & Trimble, P. J. The Atlantic multidecadal oscillation and its relation to rainfall and river flows in the continental US. *Geophys. Res. Lett.* **28**, 2077–2080 (2001).
71. Zhou, S., Miller, A. J., Wang, J. & Angell, J. K. Trends of NAO and AO and their associations with stratospheric processes. *Geophys. Res. Lett.* **28**, 4107–4110 (2001).
72. Chen, G. Revisit to atmospheric oscillations over global oceans: A combined climatology/modality approach. *Int. J. Climatol.* **34**, 2715–2729 (2014).
73. Hurrell, J. W. Decadal trends in the North Atlantic oscillation: Regional temperatures and precipitation. *Science (80-).* **269**, 676–679 (1995).
74. Schlesinger, M. E. & Ramankutty, N. An oscillation in the global climate system of period 65–70 years. *Nature* **367**, 723–726 (1994).
75. d'Orgeville, M. & Peltier, W. R. On the Pacific decadal oscillation and the Atlantic multidecadal oscillation: Might they be related? *Geophys. Res. Lett.* **34** (2007).
76. Gan, R. et al. Use of satellite leaf area index estimating evapotranspiration and gross assimilation for Australian ecosystems. *Ecohydrology* **11** (2018).
77. Leuning, R., Zhang, Y. Q., Rajaud, A., Cleugh, H. & Tu, K. A simple surface conductance model to estimate regional evaporation using MODIS leaf area index and the Penman-Monteith equation. *Water Resour. Res.* **44** (2008).
78. Zhou, H., Tang, J., Olin, S. & Miller, P. A. A comprehensive evaluation of hydrological processes in a second-generation dynamic vegetation model. *Hydrol. Process.* **38** (2024).
79. Zhang, Z., Chen, J. M., Zhang, Y. & Li, M. Improving the ability of solar-induced chlorophyll fluorescence to track gross primary production through differentiating sunlit and shaded leaves. *Agric. Meteorol.* **341**, 109658 (2023).
80. Yang, S. et al. Evaluating global ecosystem water use efficiency response to drought based on multi-model analysis. *Sci. Total Environ.* **778**, 146356 (2021).
81. Zhang, Y. et al. Multi-decadal trends in global terrestrial evapotranspiration and its components. *Sci. Rep.* **6**, 19124 (2016).
82. Mu, Q., Zhao, M. & Running, S. W. Improvements to a MODIS global terrestrial evapotranspiration algorithm. *Remote Sens. Environ.* **115**, 1781–1800 (2011).
83. Running, S. W., Mu, Q., Zhao, M. & Alvaro, M. *User's Guide MODIS Global Terrestrial Evapotranspiration (ET) Product (NASA MOD16A2/A3) NASA Earth Observing System MODIS Land Algorithm*. https://landweb.modaps.eosdis.nasa.gov/QA_WWW/forPage/user_guide/MOD16UsersGuide2016V1.52017May23.pdf (2017).
84. de Oliveira, J. V. et al. Differences in precipitation and evapotranspiration between forested and deforested areas in the Amazon rainforest using remote sensing data. *Environ. Earth Sci.* **77**, 239 (2018).
85. da Paca, V. H. The spatial variability of actual evapotranspiration across the Amazon river basin based on remote sensing products validated with flux towers. *Ecol. Process.* **8**, 6 (2019).
86. Oliveira, P. T. S. et al. Trends in water balance components across the Brazilian Cerrado. *Water Resour. Res.* **50**, 7100–7114 (2014).
87. Biudes, M. S. et al. Evapotranspiration seasonality over tropical ecosystems in Mato Grosso, Brazil. *Remote Sens.* **14**, 2482 (2022).
88. de Oliveira Serrão, E. A. et al. Hydrological processes in a watershed on the transition from Amazon to Cerrado in Brazil. *J. South. Am. Earth Sci.* **129**, 104507 (2023).
89. Baker, J. C. A. et al. Evapotranspiration in the Amazon: Spatial patterns, seasonality, and recent trends in observations, reanalysis, and climate models. *Hydrol. Earth Syst. Sci.* **25**, 2279–2300 (2021).
90. Huang, M., Zhai, P. & Piao, S. Divergent responses of ecosystem water use efficiency to drought timing over Northern Eurasia. *Environ. Res. Lett.* **16**, 045016 (2021).
91. Funk, C. et al. The climate hazards infrared precipitation with stations—a new environmental record for monitoring extremes. *Sci. Data* **2**, 150066 (2015).
92. Cavalcante, R. B. L. et al. Evaluation of extreme rainfall indices from CHIRPS precipitation estimates over the Brazilian Amazonia. *Atmos. Res.* **238**, 104879 (2020).
93. Xavier, A. C. F., Rudke, A. P., Serrão, E. A. D. O., Terassi, P. M. D. B. & Pontes, P. R. M. Evaluation of satellite-derived products for the daily average and extreme rainfall in the Mearim river drainage basin (Maranhão, Brazil). *Remote Sens.* **13**, 4393 (2021).
94. de Oliveira-Júnior, J. F. et al. Confronting CHIRPS dataset and in situ stations in the detection of wet and drought conditions in the Brazilian midwest. *Int. J. Climatol.* **41**, 4478–4493 (2021).
95. Paredes-Trejo, F. J., Barbosa, H. A. & Lakshmi Kumar, T. V. Validating CHIRPS-based satellite precipitation estimates in Northeast Brazil. *J. Arid Environ.* **139**, 26–40 (2017).
96. Jiang, F. et al. Resolving the tropical Pacific/Atlantic interaction conundrum. *Geophys. Res. Lett.* **50** (2023).
97. McKinney, W. Data structures for statistical computing in python. in 56–61. https://doi.org/10.25080/Majora-92bf1922-00a (2010).
98. Toshie Kayano, M., Valéria Andreoli, R. & de Ferreira, R. A. Evolving anomalous SST patterns leading to ENSO extremes: Relations between the tropical Pacific and Atlantic Oceans and the influence on the south American rainfall. *Int. J. Climatol.* **31**, 1119–1134 (2011).
99. Kayano, M. T. et al. Does the El Niño-Southern Oscillation affect the combined impact of the Atlantic Multidecadal Oscillation and Pacific Decadal Oscillation on the precipitation and surface air temperature variability over South America? *Atmosphere (Basel)* **13**, 231 (2022).
100. Kayano, M. T. & Capistrano, V. B. How the Atlantic multidecadal oscillation (AMO) modifies the ENSO influence on the south American rainfall. *Int. J. Climatol.* **34**, 162–178 (2014).

101. Cai, W. et al. Climate impacts of the El Niño–Southern Oscillation on South America. *Nat. Rev. Earth Environ.* **1**, 215–231 (2020).
102. Venegas, S. A., Mysak, L. A. & Straub, D. N. Atmosphere–ocean coupled variability in the South Atlantic. *J. Clim.* **10**, 2904–2920 (1997).
103. SOUZA, E. B. et al. On the influences of the El Niño, La niña and Atlantic Dipole Paterni on the amazonian rainfall during 1960–1998. *Acta Amaz.* **30**, 305–318 (2000).
104. Kousky, V. E., Kagano, M. T. & Cavalcanti, I. F. A. A review of the Southern Oscillation: Oceanic-atmospheric circulation changes and related rainfall anomalies. *Tellus Dyn. Meteorol. Oceanogr.* **36**, 490 (1984).
105. Wei, T. Simko, V. R package 'corrplot': Visualization of a correlation matrix (2021).
106. Grömping, U. Estimators of relative importance in linear regression based on variance decomposition. *Am. Stat.* **61**, 139–147 (2007).
107. Lindeman, R. H., Merenda, P. F. & Gold, R. Z. *Introduction to bivariate and multivariate analysis* (1980).

Author contributions

Edivaldo Serrão: Conceptualization, Formal analysis, Investigation, Methodology, Software, Writing - original draft, Writing - review & editing. Rosane Cavalcante: Investigation, Methodology, Project administration, Supervision, Writing - review & editing. Paulo Zanin, Renata Tedeschi and Thomás Ferreira: Data curation, Investigation, Writing - review & editing, Validation, Visualization. Paulo Pontes: Formal analysis, Funding acquisition, Project administration, Resources, Supervision, review & editing.

Declarations

Competing interests

The authors declare no competing interests.

Additional information

Supplementary Information The online version contains supplementary material available at https://doi.org/10.1038/s41598-025-85272-z.

Correspondence and requests for materials should be addressed to E.A.O.S.

Reprints and permissions information is available at www.nature.com/reprints.

Publisher's note Springer Nature remains neutral with regard to jurisdictional claims in published maps and institutional affiliations.